RSC Applied Interfaces

ROYAL SOCIETY OF CHEMISTRY

PAPER

View Article Online
View Journal | View Issue

Cite this: *RSC Appl. Interfaces*, 2026, **3**, 458

Strengthening poly(lactic acid) composites with poly(methyl methacrylate) functionalized flax nanofibrils

Abigail Mulligan,[a] Ahmad A. L. Ahmad,†[ab] Peter V. Kelly, ‡[a] Siamak Shams Es-haghi, [bc] Peng Cheng,[ab] Amber M. Hubbard, [d] Kathryn Slavny,[de] Meghan E. Lamm, [d] Sanjita Wasti[d] and William M. Gramlich *[abf]

Biobased reinforcements for poly(lactic acid) (PLA) are needed for more additive manufacturing applications requiring higher strength and sustainability. Flax nanofibrils (FNFs) produced through mechanical refining were explored as a lower energy alternative to cellulose nanofibril (CNF) reinforcements. To compatibilize the FNFs for the PLA matrix, a grafting-through surfactant free emulsion polymerization (SFEP) was performed to functionalize the FNF surface with poly(methyl methacrylate) (PMMA). FNFs produced using different refining energy were functionalized under varying solid contents in suspension. Polymerizations performed at 0.7 wt% FNFs in water yielded the highest degree of PMMA functionality. These optimal conditions were scaled up and the PMMA modified FNFs melt compounded into PLA yielding a 12% increase in tensile strength and 92% increase in the modulus of elasticity as compared to the original PLA. Interestingly, the FNFs with the lowest refining energy yielded the strongest composites using these methods, surpassing the higher refining energy CNF reinforcements. This increase was attributed to improved dispersion of the FNF reinforcements in the PLA matrix that was enabled by the PMMA coating on the FNF surface preventing interfibrillar adhesion and aggregation within the PLA matrix.

Received 4th November 2025,
Accepted 29th January 2026

DOI: 10.1039/d5lf00342c

rsc.li/RSCApplInter

Introduction

Poly(lactic acid) (PLA) has widespread use as a 3D printing[1] and packaging material due to its renewable sourcing and favorable processing conditions.[2] For example, recent work has demonstrated that biobased (wood flour) PLA composites can be used for large format additive manufacturing by printing a nearly 56 m^2 house.[3] Interest exists to add fiber reinforcements into PLA to improve its mechanical properties and reduce overall resin usage, but often these additives are non-renewable materials like glass and carbon fiber.[4] As a result, natural fibers and fibrils have been explored as alternative reinforcements.[5] However, issues can occur when attempting to melt compound these materials into PLA due to matrix-reinforcement incompatibility and incompatible processing techniques.[6] Thus, new solutions are needed to increase the available methods to incorporate natural reinforcements into PLA.

Due to their impressive individual mechanical properties, cellulose nanofibrils (CNFs) have been investigated as reinforcements for PLA composites, aiming for significant mechanical property increases at low reinforcement loadings.[7,8] Notable challenges have arisen when attempting incorporate CNFs into a PLA matrix. Typical CNF manufacturing processes occur in water that is energy intensive to remove while retaining the nanoscale properties of CNFs required for effective reinforcement.[9] Additionally, effective compatibilization between CNFs and the PLA matrix is needed for efficient dispersion and stress transfer during loading.[10] Chemical modification of the CNF surface has emerged as method to address both challenges by reducing the water–CNF interactions during drying and improving the PLA–CNF interactions during melt mixing. These past

[a] *Department of Chemistry, University of Maine, Orono, Maine 04469, USA. E-mail: william.gramlich@maine.edu*
[b] *Advanced Structures and Composites Center, University of Maine, Orono, Maine 04469, USA*
[c] *Department of Chemical and Biomedical Engineering, University of Maine, Orono, Maine 04469-5737, USA*
[d] *Manufacturing Science Division, Oak Ridge National Laboratory, Oak Ridge, Tennessee, 37830, USA*
[e] *ORISE Participant in the U.S. Department of Energy Education Collaboration at ORNL Program, Oak Ridge, Tennessee, 37830, USA*
[f] *Forest Bioproducts Research Institute, University of Maine, Orono, Maine 04469, USA*
† Current address: Department of Allied Medical Sciences, Technical College, Jadara University, Irbid, 21110, Jordan.
‡ Current address: Department of Materials Science and Engineering, Cornell University, Ithaca, New York, 14850, USA.

modification methods have relied on organic solvents and energy intensive drying methods that limit the sustainability and industrial applicability of the processes.[8,11] Completely water-based modifications can overcome these challenges[12,13] and recent work from our laboratory has demonstrated that a grafting-through surfactant free emulsion polymerization (SFEP) can retain the nanoscale properties of CNFs after industrially relevant drying methods as well as significantly increase the mechanical properties of PLA composites.[14–19]

CNFs produced through only mechanical refinement (*i.e.*, no chemical pretreatment), which are otherwise known as microfibrillated cellulose (MFC) or highly refined cellulose,[20] tend to be implemented in industry due to their lower cost.[21] However, these materials are often made from bleached kraft pulp that requires higher chemical and energy usage to produce than other pulp and fiber feedstocks.[22] One way to reduce the energy requirement is to use lignin containing feedstocks to create lignin containing CNFs (LCNFs) by forgoing chemical pulping and bleaching. Flax fibers as a source for LCNFs are particularly intriguing since they require nearly a third of the energy to produce fibers and nearly half of the energy to produce CNFs as compared to bleach softwood kraft pulp (BSKP).[23] This previous work with flax nanofibrils (FNFs) demonstrated that they can be produced with lower energy;[23] however, like CNFs, chemical modification is needed prior to compounding these materials into PLA composites as reinforcements since the same challenges around drying and compatibilization are expected.[24]

While flax fibers have been used extensively in composites, as fiber mats for epoxy resin impregnation and as additives in thermoplastic lamination and melt compounding, FNFs have been explored to a lesser extent.[25] Completely biobased flax fiber/PLA composites have been made using a multilayer compression method yielding high mechanical strength.[26–28] Unfortunately, this compression method does not enable other typical plastic processing methods like injection molding and extrusion, which can allow for added benefits like fiber alignment. Additionally, it is challenging to adapt to incorporate FNFs, since these do not form porous fiber mats easily. Flax fibers have been melt compounded into PLA[25,29] and flax fiber surface modification, which is often required for sufficient dispersion, has increased the functionality and mechanical properties of the composites.[24,30] Flax fibers have been modified with polymers but not incorporated into composites and polymer modification of FNFs has not been reported.[31] Nanoscale or highly refined flax reinforcements (FNFs) could further improve the mechanical properties of these flax composites like CNFs, but have yet to be studied in dense PLA composites, only in composite PLA foams.[32] Previous work with refined flax in poly(vinyl alcohol)[33,34] suggests that FNFs could have the same reinforcement capabilities as CNFs provided that they can be well dispersed in the matrix.

Though we have demonstrated that polymer-modified CNFs can significantly increase the mechanical properties of composites, potentially reducing the amount of material needed, the high refining energy required to produce CNFs can limit their utility.[19] FNFs have lower embodied energy and require less energy to refine than the CNFs previously used,[23] so we explored the grafting-through SFEP to improve the mechanical properties of composites through a potentially lower energy pathway. Previously reported FNFs[23] were chemically modified through a two-step modification process to coat their surface with poly(methyl methacrylate) (PMMA) through a grafting-through SFEP (Fig. 1) and compared to PMMA modified CNFs made through the same process. These previously reported FNFs and CNFs made with different refining energies were explored in this work to understand how the level of refinement affected PMMA modification and incorporation into composites. Effective reinforcements using lower refining energy could provide a lower energy and cost-effective method to create PLA reinforcements. After modification, specific surface area (SSA) and surface energetics were measured to understand how the PMMA modification affected the dried reinforcements. These PMMA–FNFs were compounded into PLA at 20 wt% loading to demonstrate whether they could act as significant reinforcements for PLA composites. Further characterization of the composites explored how the PMMA–FNFs dispersed and reinforced the composites more than CNFs made using the same reaction conditions. PMMA–FNFs made with the lowest refining energy significantly improved the mechanical properties of composites, demonstrating a lower embodied energy and higher efficiency pathway to higher strength PLA composites.

Experimental

Materials

Methyl methacrylate (MMA) at 99% purity with no further purification applied and methacrylic anhydride at 94% purity, containing 2000 ppm topanol A as an inhibitor, were purchased from Sigma Aldrich. Methylene chloride (dichloromethane, DCM), at 99.5% purity, and 99% purity potassium persulfate (KPS) were purchased from Fischer Chemical. Tetrahydrofuran was purchased from Alfa Aesar in non-UV, HPLC grade, 99.7% purity, and stabilized with 250 ppm BHT. Sodium hydroxide (NaOH) solid pellets were purchased from Fisher Chemical and diluted in reverse osmosis (RO) water to form a 10 M stock solution. Ingeo 4043D poly(lactic acid) (PLA) was purchased from NatureWorks. FNFs and CNFs were produced through a previously reported pilot-scale parallel plate refining method.[35] Information regarding the starting materials, field retted flax fibers and bleach softwood kraft pulp for FNFs and CNFs, respectively, and subsequent morphology and properties of the refined materials has been reported previously.[23,36–38] The quality of these FNFs and CNFs was reported as % fines which was determined using a Techpap

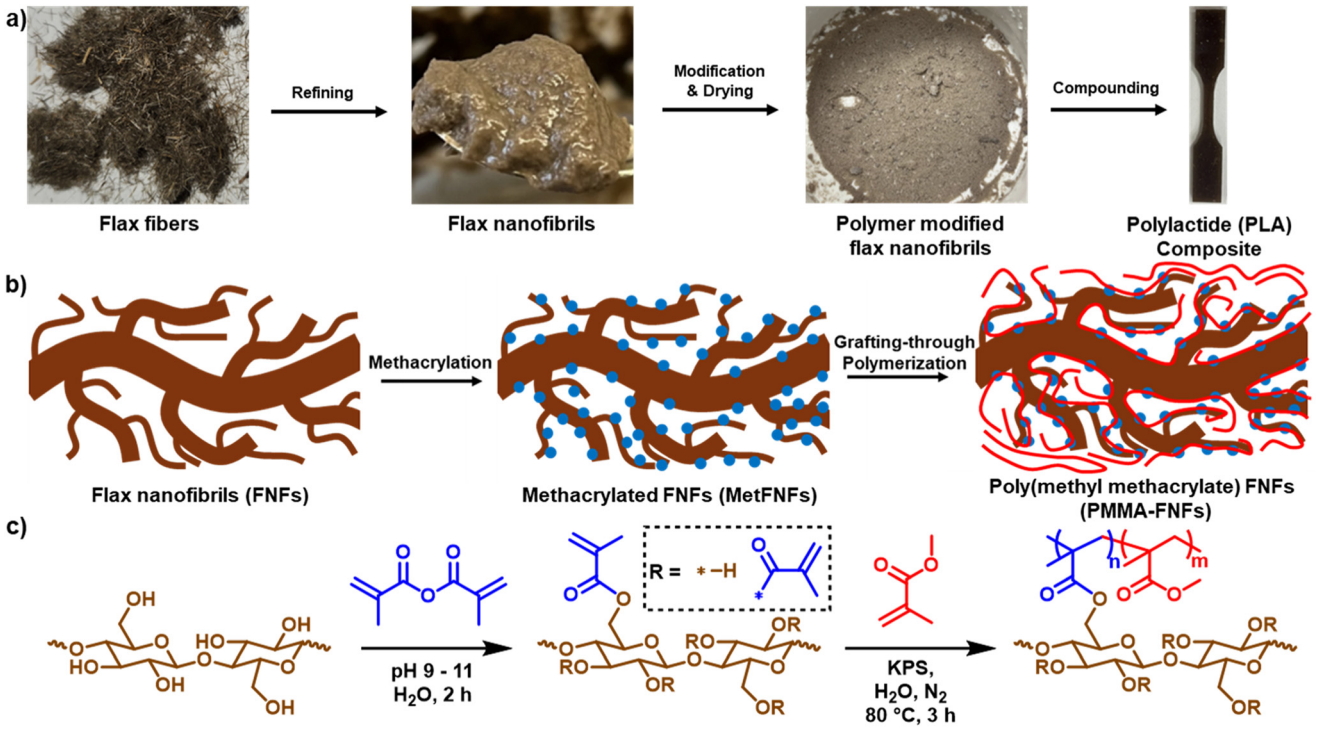

Fig. 1 a) Overview of the process to create polymer-modified flax nanofibrils (FNFs) from chopped flax fibers to be used as a polylactide (PLA) composite reinforcement. b) Schematic of the two-step modification process to generate poly(methyl methacrylate) (PMMA) functionalized FNFs (PMMA–FNFs) through a grafting-through polymerization. c) Chemical reaction scheme for the methacrylation and subsequent grafting-through polymerization of methyl methacrylate (MMA) to produce PMMA–FNFs.

Morfi compact fiber analyzer that uses a % fines definition based on the percent of total length below 200 μm.[39]

Synthesis of methacrylated FNFs (MetFNFs) and CNFs (MetCNFs)

For the methacrylation of the refined materials (Fig. 1c),[16] the as produced FNF or CNF suspension (3–4 wt% solids) was diluted in RO water to form a 1% suspension of dry mass in water. In a 5 L container, the suspension was stirred using an overhead mixer and the pH was monitored with a pH probe throughout the reaction. To the suspension, methacrylic anhydride was added to yield a 0.6 M concentration in the reaction mixture. Then, the pH of the solution was raised to 9 and maintained within a region from pH 9 to 11 through titration using a 10 M NaOH solution. These small additions of NaOH solution were made for two hours; then, the reaction was stopped by ceasing further NaOH additions and discontinuing stirring. Once stopped, the reaction mixture underwent vacuum filtration to isolate the solids. Subsequently, the product was washed five times through sequential resuspension in RO water, vigorous stirring for 3–5 minutes, and isolation through vacuum filtration. After washes four and five, the filter cake was lyophilized, and these samples were analyzed using ATR-FTIR spectroscopy (PerkinElmer ATR-FTIR Spectrum Two) to determine if the non-covalently bound methacrylates had been sufficiently washed away as indicated by no notable change in the methacrylate peak at approximately 1720 cm^{-1} in the sequential FTIR spectra. Suspensions of the purified MetFNFs and MetCNFs in water were stored at 4 °C prior to use.

Synthesis of poly(methyl methacrylate) functionalized MetFNFs (PMMA–FNFs) and MetCNFs (PMMA–CNFs)

Initially, small-scale (60 mL suspension volume) grafting-through surfactant free emulsion polymerizations (SFEPs) of MMA were performed at 0.3, 0.5, and 0.7 wt% solids of MetFNFs and MetCNFs to screen reaction conditions prior to scale up (Fig. 1c). In an example procedure, the reaction mixture was prepared by diluting 300 mg of a dry mass equivalent of MetFNFs to 60 mL of suspension with RO water to yield a 0.5 wt% MetFNF reaction mixture. The vessel was sparged with nitrogen gas for 45 minutes at room temperature while continuously stirring. The needle was removed from the suspension, but remained in the flask, and the exhaust needle was removed prior to placing the reaction vessel in an 80 °C oil bath. Once the oil bath temperature stabilized, MMA (3.2 mL) was added by needle and syringe to yield a 0.5 M concentration relative to the suspension. A new KPS stock solution in RO water (0.13 M) was prepared each time and, immediately after MMA addition, 0.26 mL of the KPS solution was injected through the septum into the reaction mixture to yield a 0.56 mM concentration relative to the suspension, starting the polymerization. The reaction

mixture was then left to polymerize while continually stirring under nitrogen for 3 hours. After, the round bottom flask was removed from the oil bath, the reaction was stopped by removing the rubber septum, exposing the reaction mixture to oxygen. Reactions at different percent solids and using MetCNFs were performed using the same conditions and amounts above except for varying the initial mass of suspension prior to dilution to reach the desired percent solids. Once stopped, the reaction mixture underwent vacuum filtration to isolate the modified solids. Subsequently, the product was washed five times through sequential resuspension in RO water, vigorous stirring for 3–5 minutes, and isolation through vacuum filtration. The solids were washed five times, and the final product was lyophilized.

To scale up to create enough reinforcement for melt compounding, the grafting-through SFEP was performed on a 10 g dry basis of the three different refining energy MetFNFs and MetCNFs at 0.7 wt% solids. The larger scale utilized a 5 L reaction vessel with an overhead stirrer with an PTFE bearing to perform the reaction under nitrogen and at 400 RPM stirring. The reaction procedures and relative ratios of reactants were the same as the small-scale reaction. One change beyond the scale and reaction vessel was the requirement for seven washes with RO water to purify the reaction product. Additionally, the products were dried in a vacuum oven at 23 °C prior to compounding and analysis.

PMMA–FNF and PMMA–CNF analysis

The dried PMMA-modified samples were analyzed using ATR-FTIR spectroscopy to determine the amount of PMMA relative to cellulose. Additionally, a small amount of the product was then suspended in DCM to remove the non-covalently bound polymer from the surface. The samples were suspended in DCM, stirred for three to five minutes, and isolated using vacuum filtration through five cycles. Then, the isolated product was dried in a vacuum oven and analyzed using ATR-FTIR spectroscopy. The water- and DCM-washed products were analyzed this way to give a total PMMA band ratio and a covalently bound PMMA band ratio, respectively. To conduct analysis, the Perkin-Elmer SpectrumTouch software was used to apply automated ATR correction, manual baseline identification and correction, and normalization of the spectra to the C3 hydroxyl band of the cellulose backbone at approximately 1055 cm^{-1}. The PMMA band height at approximately 1730 cm^{-1} was divided by the cellulose band height to calculate the band ratios.

Size exclusion chromatography (SEC) was conducted to assess the molecular weight of the non-covalently bound polymer on the surface of the MetFNFs and MetCNFs. To prepare the SEC sample, 12.5 mg of the water-washed product suspended in 1.5 mL of THF. The solution was vortexed for 30 seconds to isolate any non-covalently bound polymer from the functionalized feedstock and the solids were allowed to settle. The supernatant was passed through a 0.22 μm PTFE syringe filter prior to analysis following a previously reported procedure.[15] Following a previously reported procedure,[14] inverse gas chromatography (iGC) was performed on the scaled-up reinforcements to measure the specific surface area (SSA) as well as the dispersive component of the surface energy (γ^{d}), polar component of the surface energy (γ^{sp}), and total surface energy (γ) as a function of fractional molar surface coverage of the probe molecule (n/n_0). From these values, the work of adhesion (W_{adh}) and work of cohesion (W_{coh}) between the PMMA–FNFs and PLA as a function of fractional molar surface coverage of the probe molecule (n/n_0) were calculated following a previously reported procedure.[17,40,41] Scanning electron microscopy (SEM) was performed on the scaled-up samples by placing the dried powder on conductive tape and imaging the samples using a Hitachi TM 3000 Tabletop Microscope at 15 kV acceleration voltage.

Melt compounding and sample fabrication

Using an Intelli-Torque Plasti-Corder half size melt-mixer (Brabender), PMMA–FNF and PMMA–CNF composite materials were prepared at 5 and 20 wt% reinforcement in PLA in 28 g samples. The PLA and reinforcements were oven dried prior to compounding. The melt mixer was heated to 180 °C and PLA was added and left to melt-mix for approximately two minutes, or until the torque had stabilized. Once the torque stabilized the reinforcement was added to the molten PLA at a moderate rate to ensure even mixing. The composite was left to melt-mix until the torque stabilized again. The melt-mixer was then powered off and the material was removed from the device. Between changes in percent PMMA of the same reinforcement, no cleaning of the machine was needed. However, when changing reinforcement materials, an amount of PLA was melt-mixed to collect any contaminants from previous trials.

Following melt-mixing of the PLA and reinforcements, compression molding was conducted using a QIXING Laboratory Mini Hot Press. The melt-mixed samples were formed into a plaque with dimensions about 100 mm × 100 mm × 1.8 mm. The metallic plates were placed in the hot press, set at a temperature between 175 °C to 180 °C, where they were left to heat for 5 minutes without any pressure to further support equal distribution of the composite across the plate. After the initial 5 minutes, the pressure was gradually increased to 5 MPa and then pressed for 5 minutes. The pressure was subsequently removed, and water cooled in the press.

The composite sheets were cut to the size of the type 5 tensile molds (ASTM D638-14) and were placed over eight tensile bar molds between two metal plates. The tensile molds yielded tensile bars with an approximate thickness of 3.25 mm, a neck width of approximately 3.35 mm, and a neck length of approximately 7.26 mm. The aforementioned compression molding process was conducted once more to

mold the composite into the tensile bar molds. After the tensile bars had cooled, they were removed from their molds.

Composite analysis

Prior to tensile testing, the bars were conditioned in a 50% humidity room at a temperature of 23 °C for a minimum of 40 hours. Tensile analysis was conducted following the ASTM D638 standard and a previous procedure with an extension rate of 1.5 mm min^{-1} and using a clip-on extensometer.[16] After testing, all tensile bars were inspected for bubble defects that could have affected the tensile strength and those with such defects were removed from reporting. The rheological behavior of the composites at 5 and 20 wt% were analyzed in the linear viscoelastic region through a frequency sweep at 180 °C following previous reported methods.[14] The cross section of the composites was potted, polished and observed under the Zeiss Merlin field emission scanning electron microscope at an accelerating voltage of 1 kV after sputter coating with iridium. The detailed procedure of potting and polishing can be found elsewhere.[42] Dynamic mechanical analysis (DMA) was performed on rectangular samples with dimensions of 60 mm × 10 mm × 3 mm ($l \times w \times h$) in the viscoelastic regime from 30 to 120 °C at a temperature ramp rate of 3 °C min^{-1}, a frequency of 1 Hz, and an amplitude of 15 μm. Thermogravimetric analysis (TGA) was performed for all composite formulations where the temperature was ramped from 30 to 600 °C at a temperature ramp rate of 10 °C min^{-1} in an air environment. The temperature at which a 2 wt% mass loss was recorded as $T_{2\%}$ and the onset of thermal degradation was recorded as T_{onset}. Differential scanning calorimetry (DSC) was performed at a temperature ramp rate of 10 °C min^{-1}. The glass transition temperature (T_g), the cold crystallization temperatures (T_{cc}), and the crystallinity (X) were determined from the second heating curve for all composite formulations, as reported previously.[43,44] The density for all samples was collected according to ASTM D3576, where all tests were performed under a hydrogen environment. See SI for additional composite analysis details.

Results and discussion

Polymer-modified fibril synthesis

Both the supplied BSKP and flax were refined using a commercial production-scale disk refining process.[23] The CNFs had a standard 90% fines level while the FNFs had been produced using three different net cumulative energy (NCE) values, generating a range of % fines (Table 1). A previous publication details the different chemical and physical properties of these FNFs and CNFs.[23] Interestingly, the flax material required less than half the NCE to reach equivalent % fines than the BSKP, which is likely due to the flax fibers starting at a higher % fines as compared to the BSKP after field retting and chopping prior to refining (67% *versus* 15%, respectively).[23] Additionally, the FNFs had signals from fatty acids and lignin present in the ATR-FTIR spectra while the CNFs did not (Fig. S1).[45] In summary, the previous work using these materials demonstrated that at similar % fines, CNFs had more nanoscale structures than FNFs and the FNFs were more hydrophobic than CNFs due to their higher lignin content.[23] Thus, we expected that FNFs could have different modification behavior as compared to CNFs since the hydrophobicity of the fibrils could affect the dispersion of the fibrils in suspension (*i.e.*, increase flocculation)[37] and their ability to stabilize the hydrophobic monomer in suspension during the polymerization.[15]

After refining, both the FNFs and CNFs were reacted with methacrylic anhydride to produce FNFs and CNFs with covalently attached methacrylate groups, MetFNFs and MetCNFs, respectively (Fig. 1). While the reaction solution supernatant for the CNFs was clear, the supernatant of the FNFs during the reaction was brown, indicating that some of the lignin and other chromophores were being removed during the methacrylation process. This partial delignification is consistent with chemical retting methods[46] that use alkali conditions to liberate fibers from flax and the increased solubility of lignin under basic conditions.[47] Consequently, the FNFs transitioned from a dark orange-brown color before methacrylation to a blue-grey color after methacrylation, indicating that some lignin had been removed during the reaction and purification. The methacrylation process also appeared to remove fatty acids from the FNFs as the relative intensity of the bands corresponding to saturated C–H bonds between 2920 and 2850 cm^{-1} reduced compared to the C–O bonds at 1055 cm^{-1} in the MetFNF spectra as compared to the original FNF spectra (Fig. 2a).[45] A corresponding reduction in the carboxylic acid stretch around 1720 cm^{-1} would be expected due to the fatty acid removal; however, a band in this area still was observed due to the methacrylate functionalization forming ester linkages.

Table 1 Details of refined fiber used for grafting-through surfactant free emulsion polymerization (SFEP)

Fiber source	Refined label	NCE[a] (kWh MT^{-1})	% Fines[b]	Met : cellulose[c]
Flax	FNF-600	600	78	0.18
Flax	FNF-900	900	90	0.23
Flax	FNF-1350	1350	97	0.26
BSKP	CNF	1810	90	0.06

[a] Net cumulative energy. [b] Reported% fines.[23] [c] Band ratio of band at 1720 cm^{-1}, corresponding to C═O bond of methacrylate functionalization, and band at 1055 cm^{-1}, corresponding to the C3 C–O bond of cellulose, as a measure of degree of methacrylate substitution.

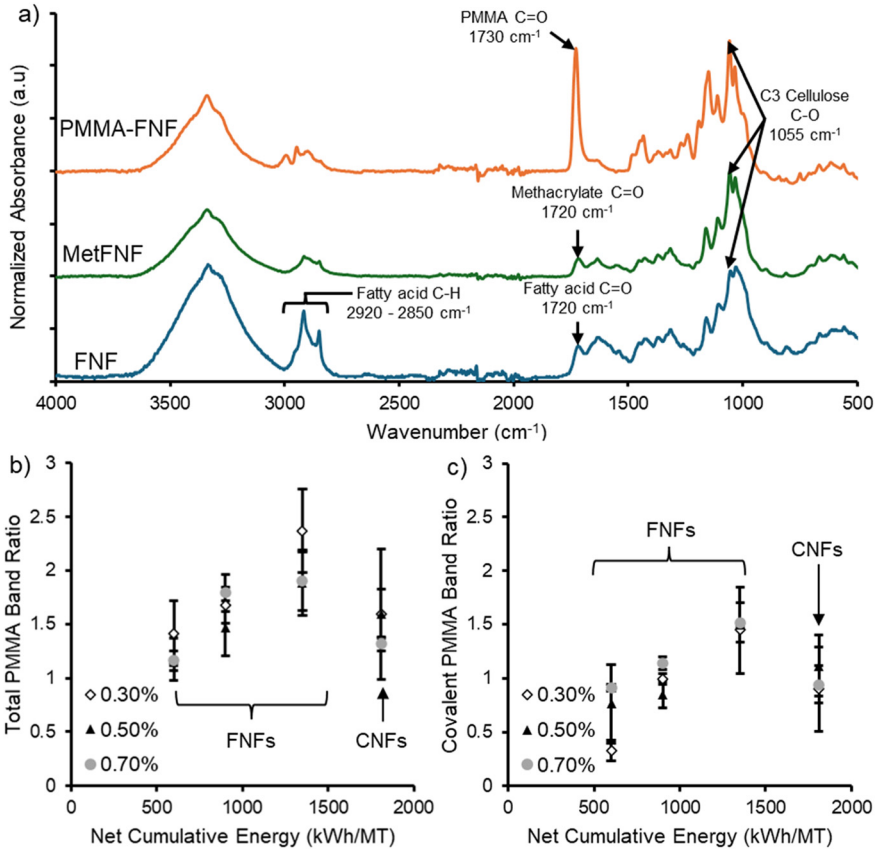

Fig. 2 a) Representative ATR-FTIR spectra of flax nanofibrils (FNFs), methacrylated FNFs (MetFNFs), and poly(methyl methacrylate) (PMMA) functionalized MetFNFs (PMMA–FNFs). Spectra have been normalized to the band at 1055 cm^{-1} and shifted vertically to improve clarity. ATR-FTIR band ratios for the band associated with PMMA carbonyl bond (*ca.* 1730 cm^{-1}) to the band associated with the C3 hydroxyl bond in cellulose (*ca.* 1055 cm^{-1}) for PMMA-modified fibrils synthesized at three different methacrylated fibril solid percents during polymerization. b) The relative band height that is proportional to the total ratio of PMMA to cellulose in the PMMA-modified materials as synthesized and washed with only water. c) The relative band height that is proportional to the covalently bound PMMA to cellulose in the PMMA-modified materials as synthesized and washed with DCM to remove the non-covalently bound PMMA, leaving covalently bound PMMA. Error bars indicate one standard deviation (n = 3).

After purification, the retention of a band around 1720 cm^{-1} in ATR-FTIR spectra, corresponding to the formation of a methacrylate ester on the fibrils (Fig. 2a), confirmed the functionalization of FNFs with methacrylates. Using the same reaction conditions, the apparent degree of methacrylation increased with increasing levels of refinement for the FNFs as indicated by the higher ratio of methacrylate to cellulose bands in the ATR-FTIR spectra (Table 1). This behavior is likely due to the increased surface area of the FNFs with higher refinement leading to more surface sites for methacrylation. The apparent functionalization of the MetCNFs as indicated by relative band heights (Table 1 and Fig. S2) was significantly lower than the MetFNFs, which could be due to the different compositions of the CNF and FNF feedstocks. The BSKP used for the CNFs had been pulped and bleached, removing much of the lignin and hemicellulose, while the flax for the FNFs had not been pulped or bleached, leaving the hemicellulose and lignin attached. The higher functionalization of the FNFs suggests that both lignin and hemicelluloses aid in the methacrylation either by aiding in the reaction to the cellulose or themselves being more reactive to the methacrylation reaction. However, this analysis is somewhat inconclusive since the fatty acid and methacrylate bands overlap in the final product and could result in an apparently higher methacrylate band due to band heights being additive.

After methacrylation, FNFs made at different refinement energies and the CNF sample were functionalized through a grafting-through surfactant free emulsion polymerization (SFEP) at three different solid contents of refined materials, 0.3, 0.5, and 0.7 wt%, while keeping the concentration of MMA and KPS initiator constant (Fig. 1). These polymerizations are known to yield polymer covalently bound to the surface of the CNFs, polymer physically adsorbed to the surface of the CNFs, and free polymer particles in suspension.[15] The fibril concentrations were varied to determine whether higher concentrations of fibrils during polymerization would increase the fraction of polymerized monomer on the surface of the resultant PMMA-modified materials *versus* the polymerized monomer in the free polymer particles. After polymerization and washing the samples with water, a new band was visible in the ATR-FTIR

spectra at around 1730 cm^{-1}, corresponding to the carbonyl groups of PMMA. This shift in wavenumber from 1720 to 1730 cm^{-1} for the carbonyl band of the methacrylate to the MMA repeat unit band is due to the loss in conjugation that is present in the original methacrylate.[48] The relative band height of this band to the cellulose backbone band at 1055 cm^{-1} was calculated to track the relative amount of PMMA to cellulose in the modified materials (Fig. 2b). For the FNFs, as the NCE increased, the amount of PMMA in the PMMA–FNFs increased, while the wt% of FNFs did not appear to affect the amount of PMMA on the fibrils. This increase can be attributed to the higher degree of methacrylation due to the increased % fines allowing for more locations for PMMA to attach to the FNF surface. Interestingly, the total amount of PMMA on the surface of the CNFs was similar to the FNF-900, with the latter having roughly half the NCE. These two samples have the same % fines, suggesting that the degree of refinement dictates the degree of PMMA modification presumably due to having similar surface areas for the polymer to attach to the surface.

Previous work has demonstrated that not all the polymerization occurs through the grafting-through process.[14–16] Polymer particles precipitate to the polymer-modified surface and polymerization occurs with monomer that adsorbs to the polymer coating the nanofibrils. Thus, covalently and non-covalently attached polymer exists on the surface of the nanomaterials. The covalently attached polymers are attached through many methacrylate links to the FNF and CNF surfaces and could not be removed from the surface for analysis.[18] However, the non-covalently bound PMMA could be removed with solvent extracted and consequently the molecular weight of the non-covalently bound polymer on the PMMA–FNFs and PMMA–CNFs was analyzed by SEC (Fig. S3). For the FNFs, as the NCE increased, the molecular weight decreased, suggesting that the available surface area affects polymerization by better emulsifying polymer particles to prevent coagulation.[49] By preventing coagulation, the surface area to volume ratio of the polymer particles increased, enabling increased diffusion of initiator into the polymer particles which increases initiation and termination within the particles to reduce the molecular weight.[49] Removal of the non-covalently attached polymer with a good solvent led to a reduction in the PMMA band relative to the cellulose band in the ATR-FTIR spectra (Fig. S4). These relative band heights for the covalently attached polymer had the same trend as the total polymer on the surface, increasing NCE for the FNFs yielded more PMMA and CNFs had similar functionalization to the same % fines FNFs (Fig. 2c). These results are consistent with the degree of grafting being controlled by the degree of refinement and thus available surface for the reaction to occur since the trends of functionalization follow the % fines of the materials.

After analysis of these small-scale experiments, we decided to scale up the reactions at 0.7 wt% for all FNFs and CNFs to produce enough materials for melt compounding in PLA. These conditions were selected because they had the lowest variability and the highest values of covalently bound polymer. This covalently bound polymer was expected to improve the adhesion between the reinforcement and PLA matrix based on previous results.[16] The larger scale syntheses had similar trends in PMMA functionalization to the small-scale reactions with increasing refining energy for the FNFs and CNFs (Table S1). Using a previously generated calibration curve to relate the band heights to PMMA and cellulose composition, we estimated that the reinforcements contained 41–48 wt% PMMA, which is consistent with previous modifications to CNFs (Table S1).[18] The amount of covalently bound PMMA was typically within the standard deviations of the small-scale reactions, while the total PMMA on the surface had differences up to 40% between the small scale and large-scale reactions. These differences can be attributed to changes in mixing geometries that somewhat alter the nature of the SFEP under shear.[50] These results demonstrate that FNF modification can be scaled up to create reinforcements without having to significantly change the reaction conditions.

Dried particle morphology and surface energetics

When the CNFs, FNFs, MetCNFs, and MetFNFs were collected by filtration and vacuum oven dried like the polymer modified reinforcements, a dense sheet of material was produced, confirming that polymer modification was required to prevent aggregation and hornification.[15,38] Conversely, the vacuum oven dried polymer modified reinforcement generated a dry powder that could be melt compounded. These PMMA–FNFs particles made through the large-scale synthesis were analyzed by iGC to understand their surface energetics after the PMMA modification. Through this process, Brunauer–Emmett–Teller (BET) theory was employed to analyze the specific surface area (SSA) of the PMMA–FNFs using *n*-octane as the probe molecule. The PMMA–CNFs could not be analyzed because their SSA was too low to generate enough surface in the sample tubes to obtain a reading. Interestingly, the SSA of the PMMA–FNFs had an inverse correlation with the NCE of refining (Fig. 3a), where PMMA–FNFs made using only 600 kWh MT^{-1} had the highest SSA of 49.5 $m^2\ g^{-1}$. As a comparison, spray dried CNFs equivalent to those used in this study had a SSA of 4.1 $m^2\ g^{-1}$.[17] This increase in SSA indicates that the PMMA modification to FNFs prevented fibrillar collapse during drying and yielded similar SSA values to PMMA–CNFs previously synthesized at 0.3 wt% (50.7 $m^2\ g^{-1}$) as opposed to the 0.7 wt% used in this study.[16] This result is a significant advancement because the PMMA–FNFs required significantly lower refining energy (600 *versus* 1810 kWh MT^{-1}) and could be produced at a higher solids content, improving chemical efficiency. The SSA of the PMMA–FNFs is equivalent to or greater than that of dried CNFs produced through typical freeze-drying processes (20–30 $m^2\ g^{-1}$) to yield "cryogels" while being vacuum dried at higher solids content (20 wt%

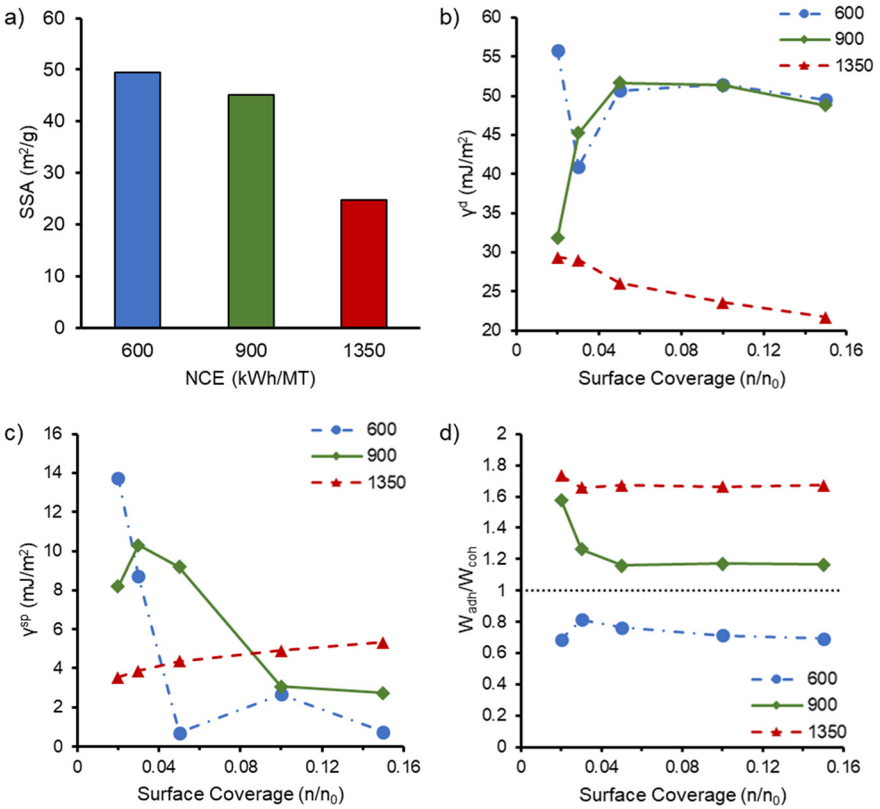

Fig. 3 a) PMMA–FNF specific surface area (SSA) by iGC as a function of net cumulative energy (NCE). b) Dispersive (γ^d) and c) polar components (γ^{sp}) of the surface energy as well as d) ratio of the work of adhesion (W_{adh}) to work of cohesion (W_{coh}) between the PMMA–FNFs and PLA as a function of fractional molar surface coverage of the probe molecule (n/n_0) for FNF refining energies of 600 (blue circles, dot-dashed line), 900 (green diamonds, solid line), and 1350 (red triangles, dashed line) kWh MT^{-1}. Connecting lines used to improve visibility. In d), the black dotted line indicates a W_{adh}/W_{coh} of 1.

versus <3 wt%), requiring less energy for water removal.[51,52] In total, these results indicate that FNFs can provide a significantly more efficient pathway to generate potential reinforcements.

Interestingly, the trend of decreasing SSA with increasing refining energy is consistent when PMMA–CNFs are considered as their SSA was too low to be measured. This behavior appears counterintuitive at first since the increased refining energy increases the % fines and presumably nanofibril content.[53] Higher nanofibril content or smaller diameter fibrils would be expected to increase the surface area of the suspension prior to modification and drying. Additionally, the more refined PMMA–FNFs typically had higher PMMA content (Table S1) which could be hypothesized to better prevent fibril collapse during drying due to the hydrophobic PMMA reducing capillary forces of the evaporating water. However, the SSA results indicate that the modification under the conditions tested is more effective at retaining the fibril morphology upon drying for the FNFs and less refined materials.

SEM images of the materials correlate with the SSA data and demonstrate that for higher refining energy the fibrils in the particles were more collapsed (Fig. 4). At low magnification, the PMMA–FNF particles at low refining energy appear more porous with fibers clearly visible. At higher magnification, fibrils are more apparent for the FNF-600 samples than for the higher refining energy samples. Following this trend, the PMMA–CNFs, which have the highest refining energy, appear to be dense ovoid structures with little space between fibers at low magnification. At higher magnification, few fibrils are observed in the dense material, which is consistent with the challenges with measuring a SSA with the iGC as little free surface area is available.

These apparently conflicting behaviors in relation to refining energy are likely related to the complex, multiphase nature of the SFEP performed. As reported for the grafting-through polymerization of styrene on MetCNFs,[15] once the initial covalently bound layer of polymer is formed on the CNFs, they become more hydrophobic causing flocculation and aggregation. Additionally, MMA has low solubility in water (150 mmol L^{-1}),[54] so it adsorbs to the PMMA-modified materials. These PMMA-coated fibrils can further stabilize larger monomer droplets, adopting the spherical shape of the monomer droplet in water. Polymerization can then proceed in this monomer swollen polymer coating, potentially crosslinking fibrils and polymerizing part of the droplet, locking the fibrils in place in a collapsed network. Higher

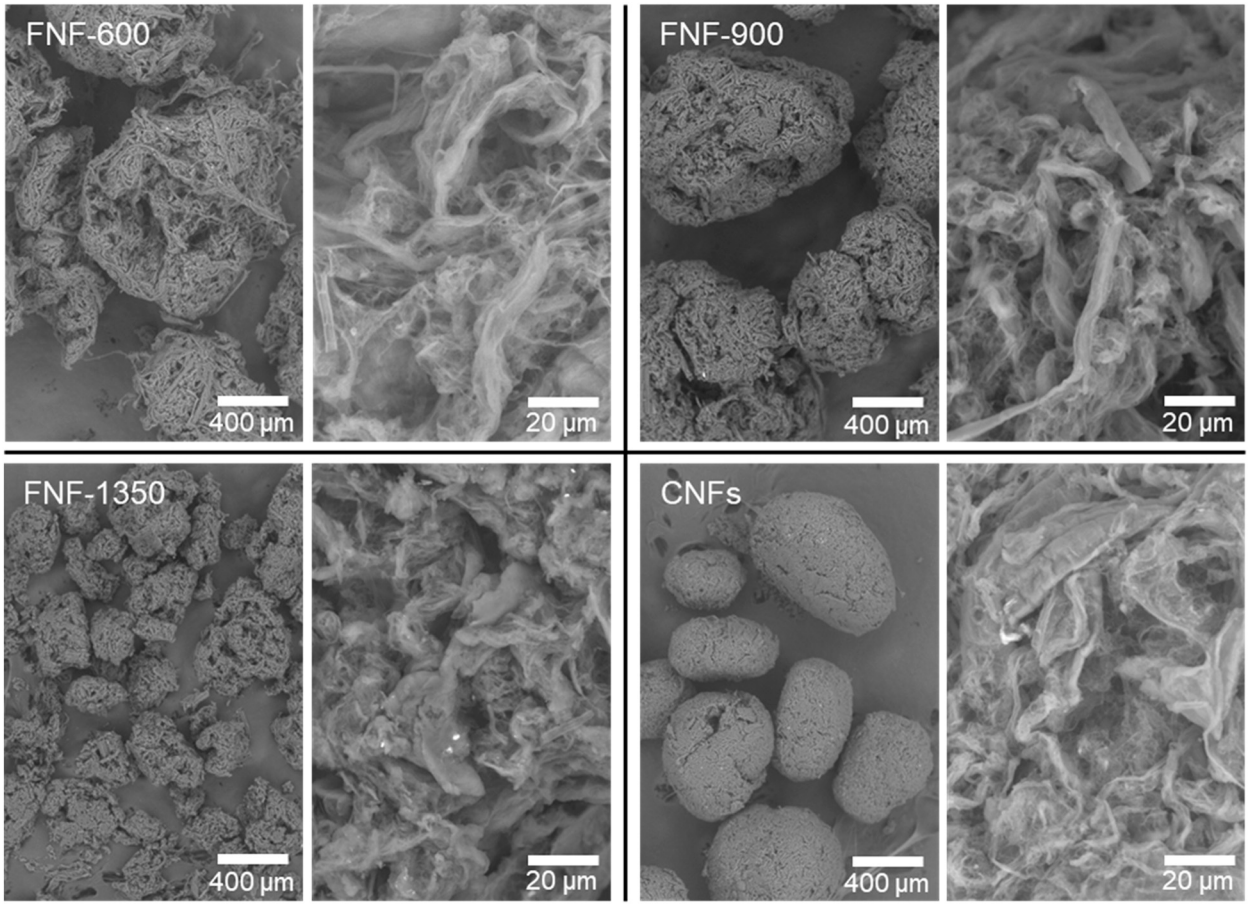

Fig. 4 Representative SEM images of PMMA–FNFs at the three refining energies (FNF-600, FNF 900, and FNF-1350 for 600, 900, and 1350 kWh MT^{-1}, respectively) and PMMA–CNFs (CNFs) at 50× (right) and 100× (left) magnification in each quadrant.

initial surface areas (*i.e.*, higher levels of refinement) would likely better stabilize the droplets initially through Pickering emulsion-like behavior and thus, could better stabilize droplets, leading to denser structures and limiting the surface area prior to drying.[55–57] This mechanism would also explain why the PMMA–CNFs had significantly lower SSA than those previously reported.[16] This reaction was performed at 0.7 wt% Met-CNFs while the previous work was done at 0.3 wt%. At the higher concentration, the fibrils would be closer together, enabling them to interact with each other and potentially allowing for crosslinking between fibrils to occur. These results demonstrate that with this grafting-through SFEP system several factors (*e.g.*, fibril concentration, substrate type) can affect the final morphology of the dried particle and should be considered with future efforts at optimization.

While the PMMA modification helped retain the fibrillar structure upon drying, it also aimed to change the surface chemistry of the FNFs and CNFs to be more compatible with the PLA matrix and thus improve mechanical properties. Measurements of surface energetics by iGC provided insight into how these modifications changed the surface chemistry of the FNFs (Fig. 3). The dispersive component of the surface energy (γ^{d}) was different between the high energy (FNF-1350) and other two PMMA–FNFs (Fig. 3b), where the FNF-1350 sample at high probe molecule surface coverage trended towards the γ^{d} of PMMA (27–40 mJ m^{-2}) suggesting that the FNFs were nearly completely coated with PMMA.[58–60] Conversely, the other two FNFs demonstrated some surface heterogeneity as the γ^{d} changed significantly with increasing probe molecule surface coverage. These higher SSA samples likely have regions that are not fully coated with PMMA leading to the probe molecule finding different binding locations at low surface coverage.[60] As the probe molecule surface coverage increased, both the FNF-600 and FNF-900 samples reached similar γ^{d} values around 50 mJ m^{-2}, which is significantly higher than PMMA and suggests incomplete coverage of the fibrils. Interestingly, this value is higher than reported values for flax fibers (35–45 mJ m^{-2})[61,62] and closer to that of CNFs (50 mJ m^{-2}).[17] These higher γ^{d} values suggest that a lower coverage of PMMA in these samples which is consistent with the measured relative degree of PMMA functionalization (Table S1).

Interestingly, the polar component of the surface energy (γ^{sp}) (Fig. 3c) has an opposite trend where the FNF-600 and FNF-900 samples had reduced values compared to the highest refining energy. The origin of this trend is not entirely clear, since it seems to contradict the γ^{d} behavior. The overall surface energy (Fig. S5) is less affected by the γ^{sp}

such that the FNF-1350 sample had a significantly lower surface energy, consistent with near total coverage with PMMA while the other two samples may have had less surface coverage that was concentrated on the more polar components. Additionally, since these two samples had higher SSA, the higher energy sites could have been more available to the probe molecules while FNF-1350 simply had these sites hidden in the collapsed fibril network.

The surface energetics analysis can also provide some potentially predictive insight into which modification will beneficially interact with the PLA matrix through comparison of the work of adhesion (W_{adh}) and work of cohesion (W_{coh}) (Fig. S5). Previous work has demonstrated that if the ratio of these two values (W_{adh}/W_{coh}) is above 1, a corresponding increase in tensile properties was observed.[37,63] Of the three refining energies, the FNF-900 and FNF-1350 samples had a W_{adh}/W_{coh} above 1, while FNF-600 did not, suggesting that these two samples could be expected to lead to improved composite properties if their dispersion within the matrix and SSA were equivalent.

Composite mechanical properties

The four reinforcements were melt compounded into PLA at two different loading levels (5 and 20 wt%) to understand how the levels of flax refining and PMMA modification affected the mechanical properties of the composite. The 5 wt% loading level was targeted to determine whether a minimal reinforcement loading could improve mechanical properties, while 20 wt% was selected because previous work with polymer modified CNFs demonstrated significant improvement at this loading.[16,17,19] These composites were compression molded into tensile bars (Fig. 5). Upon visible inspection, the CNF reinforcement did not disperse well in the composite with submillimeter scale particulates visible within the polymer matrix. These particulates are reminiscent of the CNF particles obtained after drying (Fig. 4). The composites with FNF reinforcements were much darker with a green to brown color like the original flax, indicating that lignin and pigments were still retained in the PMMA–FNFs (Fig. 5). This darkening of the PLA due to the flax makes these composites only suitable for applications where the darkness would not be a detriment such as applications that use carbon black. While some of the submillimeter scale particles were visible in the FNF composites, they appeared more uniform compared to the CNF composites, indicating improved dispersion at the macroscale. However, aggregates were still observed in the FNF composites with an apparent inverse relationship to the refining energy. The largest and most abundant agglomerates were seen in the FNF-1350

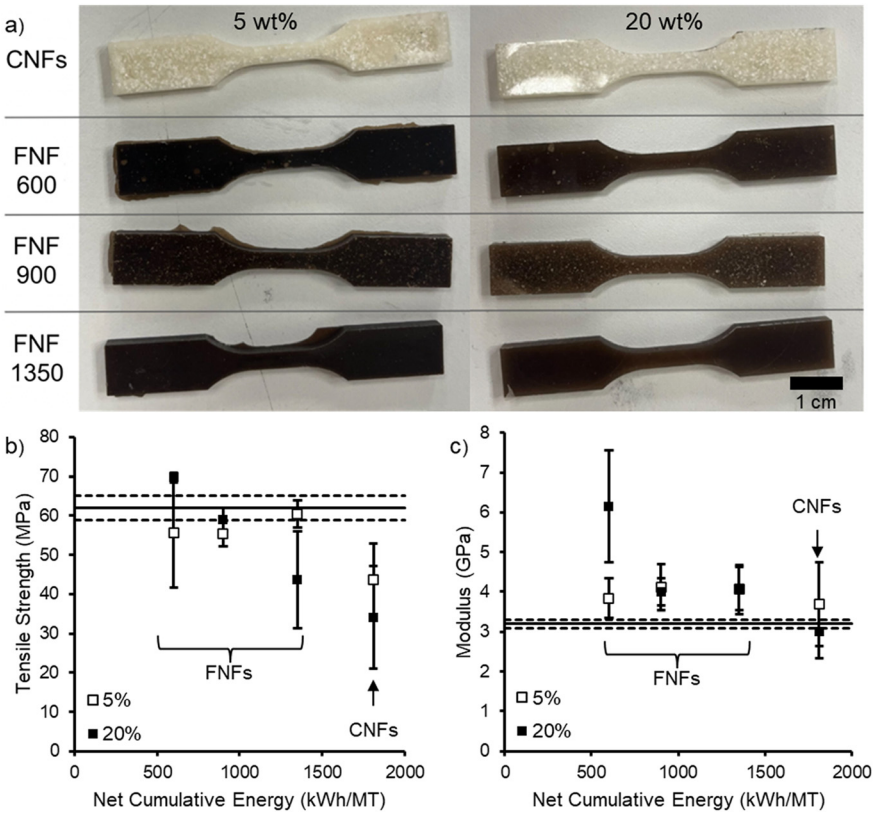

Fig. 5 a) Images of composite tensile bars with 5 (left) and 20 wt% (right) of CNF and FNF reinforcements (numbers are refining energies in kWh MT^{-1}). b) Tensile strength and c) modulus of elasticity as a function of NCE used to create the PMMA–CNFs or PMMA–FNFs compounded in PLA at 5 and 20 wt% of reinforcement. Solid lines indicate original PLA average values and dashed lines indicate error bars for PLA measurements. Error bars are one standard deviation ($n \geq 5$).

reinforced composites, subsequently leading to the most defects of the tensile bars containing the flax reinforcement. The FNF-600 reinforced composites presented with the most homogeneous appearance, with very few discrepancies in the physical appearance in the tensile bars, indicative of consistent dispersion of the reinforcement throughout the PLA matrix.

At 5 wt% FNF reinforcement loading, the tensile strength of the composites did not change significantly with increasing refining energy (Fig. 5b). These tensile strengths were similar to the original PLA (62 ± 3 MPa), indicating that the low loading did not change the composite tensile properties. Conversely, the CNF reinforcement significantly reduced the composite tensile properties at only 5 wt% loading, likely due to poor reinforcement dispersion leading to stress concentration. Increasing the reinforcement loading to 20 wt% demonstrated a decreasing trend in tensile strength with the refining NCE of FNFs. However, the composite made with FNF-600 reinforcements demonstrated a significant increase (12%, p-value = 9×10^{-5}) in tensile strength (70 ± 1 MPa) as compared to the original PLA. This reinforcement by the FNF-600 reinforcements at 20 wt% is also reflected in a substantial increase (92%) in the modulus of elasticity (Fig. 5c) from the original PLA, increasing from 3.2 ± 0.1 to 6 ± 1 GPa (p-value = 0.01), respectively. The other FNF reinforcements had modest increases in the modulus of elasticity while the CNF reinforcements did not significantly change. This significant increase in properties at 20 wt% for the FNF-600 reinforcements suggests that reinforcing network of the fibers and fibrils occurred at this weight percentage, while such a network did not develop for the other reinforcements.

Previous work with PMMA–CNFs as a reinforcement for PLA has demonstrated significant tensile strength improvements (79 ± 3 MPa, 27% increase)[16] suggesting that changes to the modification process affected the ability of the PMMA–CNFs in this study to act as a reinforcement. In the current study, the solids content was increased to 0.7 wt% from 0.3 wt% during the grafting-through SFEP while retaining the same concentration of monomer and initiator. This change appears to have led to denser PMMA–CNF particles (Fig. 4) that did not break apart and disperse well in the PLA matrix. The higher solids content could have resulted in more interfibrillar bonding and crosslinking since the fibrils would be in closer physical proximity to each other. The crosslinked PMMA–CNFs would be more difficult to break up during melt mixing. These results underscore that more work is needed to understand how the grafting-through SFEP is affected by nanofibril concentration, nanofibril structure, nanofibril chemistry, and the other reactant concentrations.

Conversely the flax-based reinforcements demonstrated mechanical property improvements at 20 wt% loading of reinforcements. Comparison of these results to literature is challenging because few examples of FNFs produced through mechanical refining or highly refined flax exist in literature.[34,64] Chemical and enzymatic treatment can yield significantly different flax nanofibril materials in terms of structure and chemistry.[65–68] Solution cast composites with flax derived nanocrystals and PLA yield significant strength improvements, but the reinforcement shape and processing methods are significantly different from those in the current study.[69] To the best of our knowledge, no reported examples exist of mechanically fibrillated flax fibers being melt compounded into PLA. However, flax fiber and PLA composites have been made through melt compounding can serve as a basis for some comparison. Oksman *et al.* demonstrated that 30 wt% of flax fiber in PLA did not significantly change the tensile strength but more than doubled the tensile modulus.[70] Similarly, Zhang *et al.* showed no change in tensile strength but a nearly 60% increase in Young's modulus for a 30 wt% flax fiber loading in PLA.[30] Silane treatment followed by precoating flax fiber with a solution of PLA in chloroform prior to melt compounding led to around a 15% increase in tensile strength and nearly doubled the modulus for a 25 wt% fiber loading in PLA.[71] Our results with PMMA–FNFs demonstrated similar improvements in tensile strength and modulus of elasticity at lower reinforcement loadings and without using organic solvents for the modification prior to melt compounding.

In comparison to the previous PMMA–CNF reinforced PLA composites, the FNF-600 reinforcements yielded a lower improvement in tensile strength (12% *versus* 27% increase), but a higher improvement in modulus of elasticity (92% *versus* 39% increase).[16] These comparisons indicate that the PMMA–FNFs can provide similar reinforcing ability to the previous PMMA–CNFs with several improvements in efficiency. First, the flax fiber has a lower embodied energy than the BSKP used to make the CNFs (*ca.* 10 *versus* 37 MJ kg^{-1}) due to its limited pretreatment and no pulping prior to refining.[23] Second, the FNFs that demonstrated the largest increase in properties required only 33% of the refining energy of the CNFs used in the previous study (600 *versus* 1810 kWh MT^{-1}). Third, the grafting-through SFEP used to make the PMMA–FNF reinforcement was run at a solids content 2.3 times greater than that of the previous PMMA–CNF reinforcement, which further improves the reaction efficiency by requiring less volume to produce the same mass of reinforcement. In total, the PMMA–FNFs provide a significantly more energy efficient pathway to create a biobased reinforcement for PLA.

Origin of mechanical property improvements

Ultimately, the physical property improvements of composites are tied to the effective dispersion of the reinforcement and the adhesion between the reinforcement and the matrix. The mechanical property improvement from FNF-600 reinforcements *versus* the other reinforcements is counter to the behavior expected from the surface energetics measurements (Fig. 3), suggesting that dispersion of the reinforcements was more significant for improvement. SEM of the composites provided some insight into the dispersion

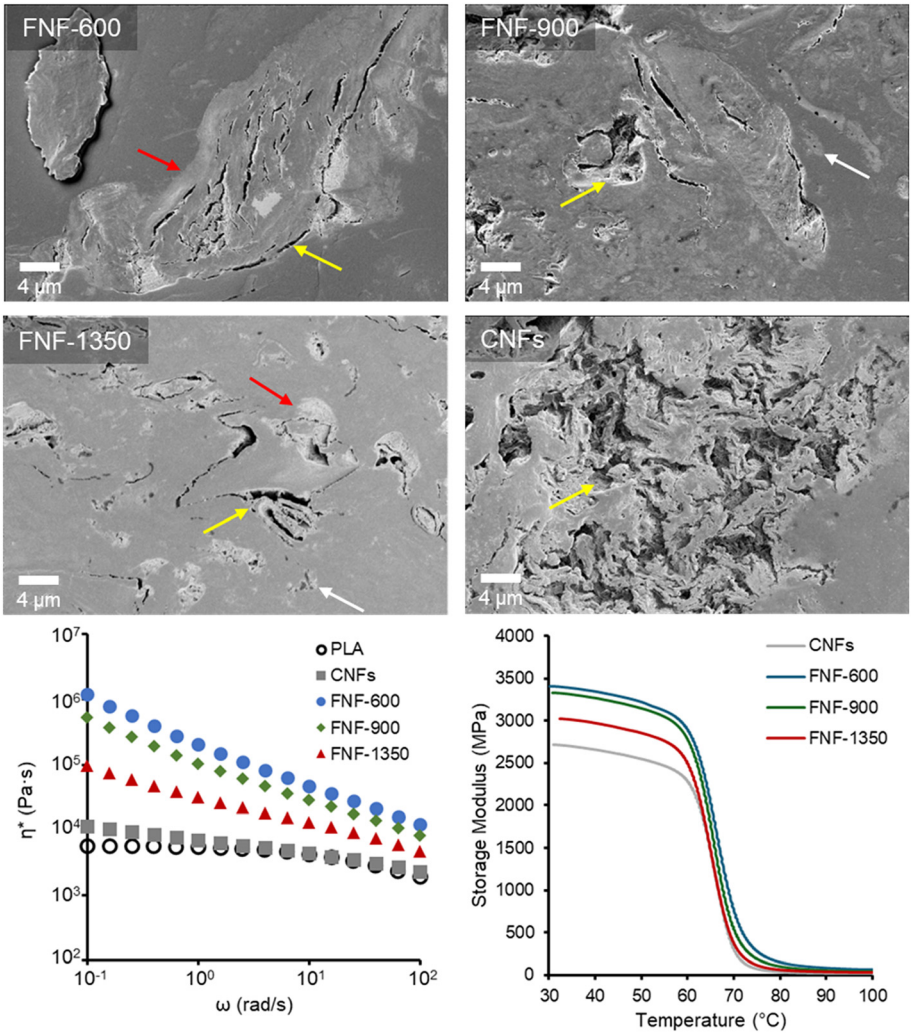

Fig. 6 (top) SEM images of composites with 20 wt% PMMA–CNF or PMMA–FNF reinforcements. Samples were polished prior to imaging. Red arrows indicate boundaries between CNF rich and polymer rich regions. White arrows indicate CNF or FNF pockets. Yellow arrows indicate air gaps and surface cracking seen within reinforcement aggregates. (bottom left) Complex viscosity (η^*) as a function of frequency (ω) at 180 °C for composites with 20 wt% PMMA–CNF or PMMA–FNF reinforcements and PLA. (bottom right) Dynamic mechanical analysis (DMA) temperature sweep for composites with 20 wt% PMMA–CNF or PMMA–FNF reinforcements.

of the reinforcements (Fig. 6). Boundaries between the reinforcements and PLA matrix are visible in all samples (red arrows, Fig. 6) at 20 wt% loading and 5 wt% loading (Fig. S7). All samples had apparent voids within the reinforcements (Fig. 6), with the CNF reinforcements having the most significant voids. At 20 wt% loading, these voids are apparently indicated in the reduced density of the composite (Fig. S8). The relative size of the voids is significantly reduced with the FNF reinforcements. These voids could be due to poor adhesion between the matrix and the reinforcements but also may be related to how the materials break up and disperse in the matrix during melt mixing. The dry FNF-600 reinforcement had the highest SSA (Fig. 3a) which indicates that the fibers and fibrils of this sample are separated from each other more than the other samples. The SEM images of the FNF-600 reinforcement also appeared to have a more open structure (Fig. 4). These results indicate that the fibers and fibrils are not as stuck together as compared to the other reinforcements. The freer fibers and fibrils likely led to the reduction in these voids during mixing through easier breakup of the reinforcement particle into individual fibrils. This improved dispersion increased both the strength and modulus of the composites. The increased presence of the voids appears to be inversely related to the mechanical properties of the composites, with larger voids indicating poor breakup of the reinforcement into fibrils within the matrix.

Since the SEM images suggested that different reinforcements had different levels of dispersion in the PLA matrix, melt rheological analysis was performed on the 20 wt% composites to elucidate the dispersion of the reinforcements. The PMMA–CNF composite had nearly the same complex viscosity behavior as the original PLA, plateauing at low frequencies (Fig. 6). Conversely, the

PMMA–FNF reinforcements demonstrated a significant increase in viscosity at low frequencies, which is consistent with the formation of a network of fibers and fibrils. The trend in the magnitude of the complex viscosity followed that of the mechanical properties with FNF-600 reinforcements having the highest value. This trend indicates that the FNF-600 reinforcements were more dispersed than the other PMMA–FNF reinforcements. This result further supports the fact that the microscopic morphology of the FNF-600 reinforcements and its more separated nature in the dry form (*e.g.*, higher SSA) is what led to it dispersing better in the matrix and significantly improving the mechanical properties. The other samples had higher PMMA content and potentially more interfibrillar linkages that hampered their breakup during melt mixing leading to worse dispersion.

The superior reinforcement of the composites with the PMMA–FNFs *versus* the PMMA–CNFs was also apparent in the DMA temperature sweep data (Fig. 6). The FNF-600 reinforcement yielded the highest storage modulus which is consistent with improved dispersion. Interestingly, at 5 wt% loading, the FNF reinforcements had nearly the equivalent storage modulus as the CNF reinforcement at 20 wt% loading (*ca.* 2700 MPa) (Fig. S9). This result further underscores how the PMMA–FNFs can be more efficient at reinforcing PLA,[19] requiring less material than PMMA–CNFs.

Addition of the reinforcements did not significantly affect the thermal stability of the materials, indicating that they did not have a detrimental effect on the PLA (Fig. S10). Furthermore, the overall crystallinity of the composites was low and did not change significantly with the inclusion of reinforcements, indicating that changes to crystallinity were not the likely cause of reinforcement (Fig. S11). Some broadening of the crystallization and melting peaks was observed in the DSC thermographs with the PMMA–FNFs *versus* the PMMA–CNFs, but it did not lead to significant changes to the cold-crystallization temperature (T_{cc}) (Fig. S11). The broadening of the crystallization and melting transitions was observed previously with highly reinforcing PMMA–CNFs in PLA and was attributed to the dispersion of the nanofibrils retarding polymer chain mobility.[16,72] These results are consistent with the improved dispersion of the PMMA–FNFs leading to the higher mechanical properties.

Conclusions

To the best of our knowledge, FNFs have not been melt compounded into compression molded PLA composites to significantly improve both their strength and modulus. To accomplish this feat, FNFs produced through mechanical refining were modified with PMMA by a grafting-through SFEP. These PMMA–FNFs better retained their high surface area after concentration and drying than PMMA–CNFs made under the same conditions, generating the highest SSA FNF reinforcements reported to date. Lower FNF refining energies led to higher SSAs in the dried PMMA–FNFs likely due to their lower nanofibril content preventing interfibrillar crosslinking during the polymerization process. This apparent reduction in interfibrillar linking and densification of the reinforcements enabled them to better break apart and disperse in the PLA matrix during melt compounding despite having lower PMMA coverage. This improved dispersion with the lowest refining energy PMMA–FNFs increased the mechanical properties of the PMMA–FNF/PLA composites. Surface energetic measurements predicted the opposite trend with higher refining energies having the most compatible interactions with PLA, but their inability to break up during shear prevented their dispersion. Thus, this study underscores the importance of both surface area and energetics to create reinforcement for composites. Additionally, the lower energy starting materials, both in terms of embodied energy and refining, combined with the higher fibril concentration SFEP provides a potentially lower cost pathway using FNFs rather than CNFs to create biobased composites for large scale additive manufacturing applications.

Author contributions

Abigail Mulligan: formal analysis, investigation, methodology, writing – original draft; Ahmad A. L. Ahmad: formal analysis, investigation, methodology; Peter V. Kelly: investigation, methodology, supervision, writing – review & editing; Siamak Shams Es-haghi: formal analysis, investigation, writing – review & editing; Peng Cheng: investigation; Amber M. Hubbard: formal analysis, investigation, visualization, supervision, writing – review & editing; Kathryn Slavny: investigation; Meghan E. Lamm: formal analysis, investigation, visualization, supervision, writing – review & editing; Sanjita Wasti: investigation; William M. Gramlich: conceptualization, formal analysis, funding acquisition, project administration, supervision, visualization, writing – original draft, writing – review & editing.

Conflicts of interest

There are no conflicts to declare.

Data availability

The data supporting this article have been included as part of the supplementary information (SI).

Supplementary information: the SI includes additional methods details, ATR-FTIR spectra, SEC data, ATR-FTIR band ratios, surface energetic data, SEM images of composites, and composite thermal data. See DOI: https://doi.org/10.1039/d5lf00342c.

Acknowledgements

This material is based upon work supported by the US Department of Energy (DOE), Office of Energy Efficiency and Renewable Energy, Advanced Materials and Manufacturing

Office under CPS Agreement 35863, and Oak Ridge National Laboratory/University of Maine SM^{2}ART program with research and resources used at the Manufacturing Demonstration Facility (MDF), a DOE AMMTO User Facility, Advanced Structures and Composites Center (ASCC), a University of Maine research center, and The Process Development Center (PDC), a University of Maine research center. This research was supported by the U.S. Department of Energy (DOE), Advanced Manufacturing Office and used resources at the Manufacturing Demonstration Facility at Oak Ridge National Laboratory (ORNL), a User Facility of DOE's Office of Energy Efficiency and Renewable Energy. This manuscript has been authored by UT-Battelle, LLC under Contract No. DE-AC05-00OR22725 with the U.S. Department of Energy. The United States Government retains and the publisher, by accepting the article for publication, acknowledges that the United States Government retains a non-exclusive, paid-up, irrevocable, world-wide license to publish or reproduce the published form of this manuscript, or allow others to do so, for United States Government purposes. The Department of Energy will provide public access to these results of federally sponsored research in accordance with the DOE Public Access Plan (http://energy.gov/downloads/doe-public-access-plan). Microscopy studies were conducted as part of a user project at the Center for Nanophase Materials Sciences, which is a US DOE Office of Science User Facility at ORNL. This research was supported in part by an appointment to the Oak Ridge National Laboratory Education Collaboration at ORNL (ECO) Program, sponsored by the U.S. Department of Energy and administered by the Oak Ridge Institute for Science and Education.

References

1 M. Lay, N. L. N. Thajudin, Z. A. A. Hamid, A. Rusli, M. K. Abdullah and R. K. Shuib, Comparison of Physical and Mechanical Properties of PLA, ABS and Nylon 6 Fabricated Using Fused Deposition Modeling and Injection Molding, *Composites, Part B*, 2019, **176**, 107341, DOI: 10.1016/j.compositesb.2019.107341.

2 A. Mehmood, N. Raina, V. Phakeenuya, B. Wonganu and K. Cheenkachorn, The Current Status and Market Trend of Polylactic Acid as Biopolymer: Awareness and Needs for Sustainable Development, *Mater. Today: Proc.*, 2023, **72**, 3049–3055, DOI: 10.1016/j.matpr.2022.08.387.

3 BioHome3D - Advanced Structures & Composites Center - University of Maine, https://composites.umaine.edu/advanced-manufacturing/biohome3d/, (accessed 2025-09-10).

4 X. Tian, T. Liu, Q. Wang, A. Dilmurat, D. Li and G. Ziegmann, Recycling and Remanufacturing of 3D Printed Continuous Carbon Fiber Reinforced PLA Composites, *J. Cleaner Prod.*, 2017, **142**, 1609–1618, DOI: 10.1016/j.jclepro.2016.11.139.

5 S. Bhagia, K. Bornani, R. Agrawal, A. Satlewal, J. Ďurkovič, R. Lagaňa, M. Bhagia, C. G. Yoo, X. Zhao, V. Kunc, Y. Pu, S. Ozcan and A. J. Ragauskas, Critical Review of FDM 3D Printing of PLA Biocomposites Filled with Biomass Resources, Characterization, Biodegradability, Upcycling and Opportunities for Biorefineries, *Appl. Mater. Today*, 2021, **24**, 101078, DOI: 10.1016/j.apmt.2021.101078.

6 A. P. Mathew, K. Oksman and M. Sain, Mechanical Properties of Biodegradable Composites from Poly Lactic Acid (PLA) and Microcrystalline Cellulose (MCC), *J. Appl. Polym. Sci.*, 2005, **97**(5), 2014–2025, DOI: 10.1002/app.21779.

7 M. Jonoobi, J. Harun, A. P. Mathew and K. Oksman, Mechanical Properties of Cellulose Nanofiber (CNF) Reinforced Polylactic Acid (PLA) Prepared by Twin Screw Extrusion, *Compos. Sci. Technol.*, 2010, **70**(12), 1742–1747, DOI: 10.1016/j.compscitech.2010.07.005.

8 H. L. Tekinalp, X. Meng, Y. Lu, V. Kunc, L. J. Love, W. H. Peter and S. Ozcan, High Modulus Biocomposites via Additive Manufacturing: Cellulose Nanofibril Networks as "Microsponges.", *Composites, Part B*, 2019, **173**, 106817, DOI: 10.1016/j.compositesb.2019.05.028.

9 Y. Peng, D. J. Gardner and Y. Han, Drying Cellulose Nanofibrils: In Search of a Suitable Method, *Cellulose*, 2012, **19**(1), 91–102, DOI: 10.1007/s10570-011-9630-z.

10 L. Zhou, K. Ke, M.-B. Yang and W. Yang, Recent Progress on Chemical Modification of Cellulose for High Mechanical-Performance Poly(Lactic Acid)/Cellulose Composite: A Review, *Compos. Commun.*, 2021, **23**, 100548, DOI: 10.1016/j.coco.2020.100548.

11 C. M. Clarkson, S. M. El Awad Azrak, R. Chowdhury, S. N. Shuvo, J. Snyder, G. Schueneman, V. Ortalan and J. P. Youngblood, Melt Spinning of Cellulose Nanofibril/Polylactic Acid (CNF/PLA) Composite Fibers For High Stiffness, *ACS Appl. Polym. Mater.*, 2019, **1**(2), 160–168, DOI: 10.1021/acsapm.8b00030.

12 S. Spinella, C. Samuel, J.-M. Raquez, S. A. McCallum, R. Gross and P. Dubois, Green and Efficient Synthesis of Dispersible Cellulose Nanocrystals in Biobased Polyesters for Engineering Applications, *ACS Sustainable Chem. Eng.*, 2016, **4**(5), 2517–2527, DOI: 10.1021/acssuschemeng.5b01611.

13 N. Macke, C. M. Hemmingsen and S. J. Rowan, The Effect of Polymer Grafting on the Mechanical Properties of PEG-Grafted Cellulose Nanocrystals in Poly(Lactic Acid), *J. Polym. Sci.*, 2022, **60**(24), 3318–3330, DOI: 10.1002/pol.20220127.

14 A. A. L. Ahmad, S. Shams Es-haghi and W. M. Gramlich, Enhancing Poly(Lactic Acid) Composites with Polymer-Modified Bleached Softwood Kraft Pulp Before and After Fibrillation, *ACS Appl. Polym. Mater.*, 2024, **6**(20), 12575–12584, DOI: 10.1021/acsapm.4c02149.

15 M. E. Driscoll, P. V. Kelly and W. M. Gramlich, Impact of Aqueous Grafting of Polystyrene through Methacrylate-Modified Cellulose Nanofibrils on Emulsion Stabilization and Drying Behavior, *Langmuir*, 2023, **39**(20), 7079–7090, DOI: 10.1021/acs.langmuir.3c00321.

16 H. Senkum, P. V. Kelly, A. A. L. Ahmad, S. Shams Es-haghi and W. M. Gramlich, Strengthening Polylactic Acid (PLA) Composites with Poly(Methyl Methacrylate)-Functionalized Cellulose Nanofibrils Created through Grafting-through Emulsion Polymerization, *RSC Appl. Polym.*, 2024, **2**(2), 224–237, DOI: 10.1039/D3LP00248A.

17 P. V. Kelly, S. Shams Es-haghi, M. E. Lamm, K. Copenhaver, S. Ozcan, D. J. Gardner and W. M. Gramlich, Polymer-Grafted Cellulose Nanofibrils with Enhanced Interfacial Compatibility for Stronger Poly(Lactic Acid) Composites, *ACS Appl. Polym. Mater.*, 2023, **5**(5), 3661–3676, DOI: 10.1021/acsapm.3c00312.

18 P. V. Kelly, P. Cheng, D. J. Gardner and W. M. Gramlich, Aqueous Polymer Modification of Cellulose Nanofibrils by Grafting-Through a Reactive Methacrylate Group, *Macromol. Rapid Commun.*, 2021, **42**(3), 2000531, DOI: 10.1002/marc.202000531.

19 P. V. Kelly, S. Shams Es-haghi, A. A. L. Ahmad, M. E. Lamm, K. Copenhaver, E. Alyamac-Seydibeyoglu, S. Ozcan, D. J. Gardner and W. M. Gramlich, High-Strength 3D Printed Poly(Lactic Acid) Composites Reinforced by Shear-Aligned Polymer-Grafted Cellulose Nanofibrils, *RSC Appl. Polym.*, 2025, **3**(1), 111–124, DOI: 10.1039/d4lp00283k.

20 V. Kumar, R. Bollström, A. Yang, Q. Chen, G. Chen, P. Salminen, D. Bousfield and M. Toivakka, Comparison of Nano- and Microfibrillated Cellulose Films, *Cellulose*, 2014, **21**(5), 3443–3456, DOI: 10.1007/s10570-014-0357-5.

21 M. Ankerfors, T. Lindström and D. Söderberg, The Use of Microfibrillated Cellulose in Fine Paper Manufacturing – Results from a Pilot Scale Papermaking Trial, *Nord. Pulp Pap. Res. J.*, 2014, **29**(3), 476–483, DOI: 10.3183/npprj-2014-29-03-p476-483.

22 K. Copenhaver, K. Li, L. Wang, M. Lamm, X. Zhao, M. Korey, D. Neivandt, B. Dixon, S. Sultana, P. Kelly, W. M. Gramlich, H. Tekinalp, D. J. Gardner, S. MacKay, K. Nawaz and S. Ozcan, Pretreatment of Lignocellulosic Feedstocks for Cellulose Nanofibril Production, *Cellulose*, 2022, **29**(9), 4835–4876, DOI: 10.1007/s10570-022-04580-z.

23 M. E. Lamm, D. A. Johnson, K. Copenhaver, S. Bhagia, A. M. Hubbard, C. C. Walker, K. Doyle and S. Ozcan, Exploiting the Properties of Non-Wood Feedstocks to Produce Tailorable Lignin-Containing Cellulose Nanofibers, *Polymers*, 2024, **16**(18), 2598, DOI: 10.3390/polym16182598.

24 X. Xia, W. Liu, L. Zhou, Z. Hua, H. Liu and S. He, Modification of Flax Fiber Surface and Its Compatibilization in Polylactic Acid/Flax Composites, *Iran. Polym. J.*, 2016, **25**(1), 25–35, DOI: 10.1007/s13726-015-0395-3.

25 I. Taha and G. Ziegmann, A Comparison of Mechanical Properties of Natural Fiber Filled Biodegradable and Polyolefin Polymers, *J. Compos. Mater.*, 2006, **40**, 1933–1946, DOI: 10.1177/0021998306061304.

26 E. Bodros, I. Pillin, N. Montrelay and C. Baley, Could Biopolymers Reinforced by Randomly Scattered Flax Fibre Be Used in Structural Applications?, *Compos. Sci. Technol.*, 2007, **67**(3), 462–470, DOI: 10.1016/j.compscitech.2006.08.024.

27 B. Bax and J. Müssig, Impact and Tensile Properties of PLA/Cordenka and PLA/Flax Composites, *Compos. Sci. Technol.*, 2008, **68**(7), 1601–1607, DOI: 10.1016/j.compscitech.2008.01.004.

28 A. Couture, G. Lebrun and L. Laperrière, Mechanical Properties of Polylactic Acid (PLA) Composites Reinforced with Unidirectional Flax and Flax-Paper Layers, *Compos. Struct.*, 2016, **154**, 286–295, DOI: 10.1016/j.compstruct.2016.07.069.

29 B. Bax and J. Müssig, Impact and Tensile Properties of PLA/Cordenka and PLA/Flax Composites, *Compos. Sci. Technol.*, 2008, **68**(7), 1601–1607, DOI: 10.1016/j.compscitech.2008.01.004.

30 L. Zhang, Z. Li, Y.-T. Pan, A. P. Yáñez, S. Hu, X.-Q. Zhang, R. Wang and D.-Y. Wang, Polydopamine Induced Natural Fiber Surface Functionalization: A Way towards Flame Retardancy of Flax/Poly(Lactic Acid) Biocomposites, *Composites, Part B*, 2018, **154**, 56–63, DOI: 10.1016/j.compositesb.2018.07.037.

31 B. S. Kaith and S. Kalia, Synthesis and Characterization of Graft Co-Polymers of Flax Fiber with Binary Vinyl Monomers, *Int. J. Polym. Anal. Charact.*, 2007, **12**(5), 401–412, DOI: 10.1080/10236660701543676.

32 M. Bulota and T. Budtova, Highly Porous and Light-Weight Flax/PLA Composites, *Ind. Crops Prod.*, 2015, **74**, 132–138, DOI: 10.1016/j.indcrop.2015.04.045.

33 E. H. Qua, P. R. Hornsby, H. S. S. Sharma, G. Lyons and R. D. McCall, Preparation and Characterization of Poly(Vinyl Alcohol) Nanocomposites Made from Cellulose Nanofibers, *J. Appl. Polym. Sci.*, 2009, **113**(4), 2238–2247, DOI: 10.1002/app.30116.

34 A. Bhatnagar and M. Sain, Processing of Cellulose Nanofiber-Reinforced Composites, *J. Reinf. Plast. Compos.*, 2005, **24**(12), 1259–1268, DOI: 10.1177/0731684405049864.

35 M. A. Bilodeau and M. A. Paradis, High Efficiency Production of Nanofibrillated Cellulose, US9988762B2, June 5, 2018, https://patents.google.com/patent/US9988762B2/en, (accessed 2025-09-04).

36 S. Christau, E. Alyamac-Seydibeyoglu, K. Thayer and W. M. Gramlich, Effects of an Aqueous Surface Modification via a Grafting-through Polymerization Approach on the Fibrillation and Drying of Bleached Softwood Kraft Pulp, *Cellulose*, 2023, **30**(2), 901–914, DOI: 10.1007/s10570-022-04938-3.

37 P. V. Kelly, D. J. Gardner and W. M. Gramlich, Optimizing Lignocellulosic Nanofibril Dimensions and Morphology by Mechanical Refining for Enhanced Adhesion, *Carbohydr. Polym.*, 2021, **273**, 118566, DOI: 10.1016/j.carbpol.2021.118566.

38 A. A. L. Ahmad and W. M. Gramlich, Methacrylate and Polymer Grafting Pulp Pretreatments Reduce Refining Energy to Produce Modified Cellulose Nanofibrils, *Cellulose*, 2024, **31**, 2865–2880, DOI: 10.1007/s10570-024-05796-x.

39 D. Guay, N. R. Sutherland, W. Rantanen, N. Malandri, A. Stephens, K. Mattingly and M. Schneider, Comparison of Fiber Length Analyzers, 2005 TAPPI Practical Papermaking Conference [electronic resource]: May 22–26, 2005, Milwaukee, Wisconsin, Atlanta, GA: Tappi Press, c2005: ISBN: 1595100946: 9781595100948: [30] pages, 2005.

40 D. J. Burnett, J. Khoo, M. Naderi, J. Y. Y. Heng, G. D. Wang and F. Thielmann, Effect of Processing Route on the Surface Properties of Amorphous Indomethacin Measured by Inverse Gas Chromatography, *AAPS PharmSciTech*, 2012, **13**(4), 1511–1517, DOI: 10.1208/s12249-012-9881-5.

41 K. Adamska, M. Sandomierski, Z. Buchwald and A. Voelkel, Inverse Gas Chromatography in the Examination of Surface Properties of Experimental Dental Composites, *Polym. Test.*, 2020, **90**, 106697, DOI: 10.1016/j.polymertesting.2020.106697.

42 S. I. Talabi, K. Chawla, B. Rodriguez, A. Barakat, Y. Meraki, A. Phadatare, M. Brander, B. Šeta, J. Spangenberg, H. F. Wu, U. Vaidya, V. Kunc, A. A. Hassen and V. Kumar, Fiber Orientation and Porosity in Large-Format Extrusion Process: The Role of Processing Parameters, *Composites, Part A*, 2025, **194**, 108891, DOI: 10.1016/j.compositesa.2025.108891.

43 A. M. Hubbard, K. Copenhaver, C. M. Clarkson, A. M. Rossy, M. L. Rencheck, M. E. Lamm and S. Ozcan, Creep Suppression and Fatigue in Bio-Based Composites Manufactured via Conventional and Large Format Additive Manufacturing Processes, *Next Mater.*, 2025, **9**, 100940, DOI: 10.1016/j.nxmate.2025.100940.

44 S. Wasti, A. M. Hubbard, C. M. Clarkson, E. Johnston, H. Tekinalp, S. Ozcan and U. Vaidya, Long Coir and Glass Fiber Reinforced Polypropylene Hybrid Composites Prepared via Wet-Laid Technique, *Compos., Part C: Open Access*, 2024, **14**, 100445, DOI: 10.1016/j.jcomc.2024.100445.

45 D. S. Himmelsbach, S. Khalili and D. E. Akin, The Use of FT-IR Microspectroscopic Mapping to Study the Effects of Enzymatic Retting of Flax (Linum Usitatissimum L) Stems, *J. Sci. Food Agric.*, 2002, **82**(7), 685–696, DOI: 10.1002/jsfa.1090.

46 A. P. S. Adamsen, D. E. Akin and L. L. Rigsby, Chemical Retting of Flax Straw Under Alkaline Conditions, *Text. Res. J.*, 2002, **72**(9), 789–794, DOI: 10.1177/004051750207200907.

47 E. I. Evstigneyev and S. M. Shevchenko, Structure, Chemical Reactivity and Solubility of Lignin: A Fresh Look, *Wood Sci. Technol.*, 2019, **53**(1), 7–47, DOI: 10.1007/s00226-018-1059-1.

48 R. S. Rasmussen and R. R. Brattain, Infrared Spectra of Some Carboxylic Acid Derivatives, *J. Am. Chem. Soc.*, 1949, **71**(3), 1073–1079, DOI: 10.1021/ja01171a088.

49 T. Tanrisever, O. Okay and I. Ç. Sönmezoğlu, Kinetics of Emulsifier–Free Emulsion Polymerization of Methyl Methacrylate, *J. Appl. Polym. Sci.*, 1996, **61**(3), 485–493, DOI: 10.1002/(SICI)1097-4628(19960718)61:3%253C485::AID-APP11%253E3.0.CO;2-0.

50 Y. Shi, G. Shan and Y. Shang, Role of Poly(Ethylene Glycol) in Surfactant-Free Emulsion Polymerization of Styrene and Methyl Methacrylate, *Langmuir*, 2013, **29**(9), 3024–3033, DOI: 10.1021/la304847a.

51 C. Darpentigny, G. Nonglaton, J. Bras and B. Jean, Highly Absorbent Cellulose Nanofibrils Aerogels Prepared by Supercritical Drying, *Carbohydr. Polym.*, 2020, **229**, 115560, DOI: 10.1016/j.carbpol.2019.115560.

52 M. Pääkkö, J. Vapaavuori, R. Silvennoinen, H. Kosonen, M. Ankerfors, T. Lindström, L. A. Berglund and O. Ikkala, Long and Entangled Native Cellulose I Nanofibers Allow Flexible Aerogels and Hierarchically Porous Templates for Functionalities, *Soft Matter*, 2008, **4**(12), 2492–2499, DOI: 10.1039/B810371B.

53 E. E. O'Banion and S. Shams Es-haghi, Rheological Behavior of Cellulose Nanofibril Suspensions with Varied Levels of Fines and Solid Content, *Polymer*, 2023, **288**, 126445, DOI: 10.1016/j.polymer.2023.126445.

54 M. J. Ballard, D. H. Napper and R. G. Gilbert, Kinetics of Emulsion Polymerization of Methyl Methacrylate, *J. Polym. Sci., Polym. Chem. Ed.*, 1984, **22**(11), 3225–3253, DOI: 10.1002/pol.1984.170221141.

55 S. Fujisawa, Material Design of Nanocellulose/Polymer Composites via Pickering Emulsion Templating, *Polym. J.*, 2021, **53**(1), 103–109, DOI: 10.1038/s41428-020-00408-4.

56 S. Fujisawa, E. Togawa and K. Kuroda, Facile Route to Transparent, Strong, and Thermally Stable Nanocellulose/Polymer Nanocomposites from an Aqueous Pickering Emulsion, *Biomacromolecules*, 2017, **18**(1), 266–271, DOI: 10.1021/acs.biomac.6b01615.

57 N. Nikfarjam, N. Taheri Qazvini and Y. Deng, Surfactant Free Pickering Emulsion Polymerization of Styrene in w/o/w System Using Cellulose Nanofibrils, *Eur. Polym. J.*, 2015, **64**, 179–188, DOI: 10.1016/j.eurpolymj.2015.01.007.

58 M. M. Chehimi, M.-L. Abel, C. Perruchot, M. Delamar, S. F. Lascelles and S. P. Armes, The Determination of the Surface Energy of Conducting Polymers by Inverse Gas Chromatography at Infinite Dilution, *Synth. Met.*, 1999, **104**(1), 51–59, DOI: 10.1016/S0379-6779(99)00040-5.

59 B. Riedl and P. D. Kamdem, Estimation of the Dispersive Component of Surface Energy of Polymer-Grafted Lignocellulosic Fibers with Inverse Gas Chromatography, *J. Adhes. Sci. Technol.*, 1992, **6**(9), 1053–1067, DOI: 10.1163/156856192X00935.

60 M. Ahmadi, T. Behzad, R. Bagheri, M. Ghiaci and M. Sain, Topochemistry of Cellulose Nanofibers Resulting from Molecular and Polymer Grafting, *Cellulose*, 2017, **24**(5), 2139–2152, DOI: 10.1007/s10570-017-1254-5.

61 J. Y. Y. Heng, D. F. Pearse, F. Thielmann, T. Lampke and A. Bismarck, Methods to Determine Surface Energies of Natural Fibres: A Review, *Compos. Interfaces*, 2007, **14**(7–9), 581–604, DOI: 10.1163/156855407782106492.

62 G. Cantero, A. Arbelaiz, R. Llano-Ponte and I. Mondragon, Effects of Fibre Treatment on Wettability and Mechanical Behaviour of Flax/Polypropylene Composites, *Compos. Sci. Technol.*, 2003, **63**(9), 1247–1254, DOI: 10.1016/S0266-3538(03)00094-0.

63 G. S. Oporto, D. J. Gardner, A. Kiziltas and D. J. Neivandt, Understanding the Affinity between Components of Wood–Plastic Composites from a Surface Energy Perspective, *J. Adhes. Sci. Technol.*, 2011, **25**(15), 1785–1801, DOI: 10.1163/016942410X525759.

64 E. H. Qua, P. R. Hornsby, H. S. S. Sharma and G. Lyons, Preparation and Characterisation of Cellulose Nanofibres, *J. Mater. Sci.*, 2011, **46**(18), 6029–6045, DOI: 10.1007/s10853-011-5565-x.

65 H. Nlandu, K. Belkacemi, N. Chorfa, S. Elkoun, M. Robert and S. Hamoudi, Flax Nanofibrils Production via Supercritical Carbon Dioxide Pre-Treatment and Enzymatic Hydrolysis, *Can. J. Chem. Eng.*, 2020, **98**(1), 84–95, DOI: 10.1002/cjce.23596.

66 H. Nlandu, K. Belkacemi, N. Chorfa, S. Elkoun, M. Robert and S. Hamoudi, Laccase-Mediated Grafting of Phenolic Compounds onto Lignocellulosic Flax Nanofibers, *J. Nat. Fibers*, 2022, **19**(1), 222–231, DOI: 10.1080/15440478.2020.1738307.

67 W. Chen, H. Yu, Y. Liu, Y. Hai, M. Zhang and P. Chen, Isolation and Characterization of Cellulose Nanofibers from

Four Plant Cellulose Fibers Using a Chemical-Ultrasonic Process, *Cellulose*, 2011, **18**(2), 433–442, DOI: 10.1007/s10570-011-9497-z.

68 S. Alila, I. Besbes, M. R. Vilar, P. Mutjé and S. Boufi, Non-Woody Plants as Raw Materials for Production of Microfibrillated Cellulose (MFC): A Comparative Study, *Ind. Crops Prod.*, 2013, **41**, 250–259, DOI: 10.1016/j.indcrop.2012.04.028.

69 D. Y. Liu, X. W. Yuan, D. Bhattacharyya and A. J. Easteal, Characterisation of Solution Cast Cellulose Nanofibre – Reinforced Poly(Lactic Acid), *eXPRESS Polym. Lett.*, 2010, **4**(1), 26–31, DOI: 10.3144/expresspolymlett.2010.5.

70 K. Oksman, M. Skrifvars and J.-F. Selin, Natural Fibres as Reinforcement in Polylactic Acid (PLA) Composites, *Compos. Sci. Technol.*, 2003, **63**(9), 1317–1324, DOI: 10.1016/S0266-3538(03)00103-9.

71 M. Kodal, Z. D. Topuk and G. Ozkoc, Dual Effect of Chemical Modification and Polymer Precoating of Flax Fibers on the Properties of Short Flax Fiber/Poly(Lactic Acid) Composites, *J. Appl. Polym. Sci.*, 2015, **132**(48), 42564, DOI: 10.1002/app.42564.

72 J. Kratochvíl and I. Kelnar, Non-Isothermal Kinetics of Cold Crystallization in Multicomponent PLA/Thermoplastic Polyurethane/Nanofiller System, *J. Therm. Anal. Calorim.*, 2017, **130**(2), 1043–1052, DOI: 10.1007/s10973-017-6417-y.